Journal of Computers Vol. 36 No. 5, October 2025, pp. 363-378
https://doi.org/10.63367/19911599202510360502 4

Development of Dynamic and Static Performance Testing System for Servo Control Valve Based on Digital Twins and Intelligent Fault Diagnosis Strategy

Jian-Rong Dong[1,2*], Zhong-Min Yin[1], Li-Ming Ma[1],
Hui-Juan Cui[3], and Bo Liu[4]

[1] Hebei Institute of Mechanical and Electrical Technology,
Xingtai City 054000, Hebei Province, China
01291979@163.com, 332908177@qq.com, maliming100@126.com

[2] Xingtai Metal Processing Equipment Intelligent Integration and Diagnosis Technology Innovation Center
Xingtai City 054000, Hebei Province, China

[3] Xianyang Polytechnic Institute, Xi'an City 712000, Shanxi Province, China
252680385@qq.com

[4] Tangshan Polytechnic University,
Tangshan City 063299, Hebei Province, China
liubo20230101@163.com

Received 1 August 2025; Revised 22 September 2025; Accepted 7 October 2025

Abstract. This article focuses on the dynamic and static performance testing of hydraulic servo control valves and the problem of valve fault detection. Firstly, the framework of digital twin is sorted out and proposed. Digital twin is the end link of the detection system and the fault diagnosis system. The digital twin framework explains the construction scheme of the framework, which includes intelligent diagnosis function for servo valve faults. For the intelligent diagnosis method, this article uses the fault diagnosis algorithm of CNN-LSTM to fully extract the fault characteristics of the input sequence as the input of LSTM, relying on LSTM to fully capture the temporal characteristics of the servo valve. Finally, in the conclusion section, the implementation scheme of the overall framework is given, and the feasibility and effectiveness of the intelligent diagnosis algorithm are analyzed.

Keywords: electro hydraulic servo valve, dynamic and static performance, fault diagnosis algorithm, digital twin

1 Introduction

In recent years, due to its ability to control and transfer energy, enhance mechanical efficiency and transmission, hydraulic technology has become one of the main components of automated, high-speed, and high-precision mechanical systems, and is widely used in industrial production's engineering machinery, aerospace, military and other fields. Hydraulic components are a key part that affects the level of hydraulic technology and are used to regulate the direction, pressure, and flow of fluid in fluid transmission circuits. Servo valve is a hydraulic component that converts electrical signals into hydraulic signals to achieve flow output or pressure control. Its types include nozzle baffle servo valve, jet pipe servo valve, and deflection plate jet servo valve. Hydraulic systems typically include electrical modules and hydraulic modules, with hydraulic servo valves serving as a bridge between the two. Their function is to proportionally convert low-power electrical signals into high-power hydraulic energy, thereby achieving control over the hydraulic circuit. Therefore, the performance of servo valves will directly affect the control accuracy, response speed, reliability, and lifespan of the entire hydraulic control system. Hydraulic servo valves are mainly composed of three parts: electric mechanical actuators, hydraulic amplifiers, and feedback mechanisms. Hydraulic amplifiers are also known as hydraulic control valves, which convert mechanical motion into high-power hydraulic energy output. The power stage main valve of hydraulic servo valves

* Corresponding Author

mainly adopts slide valve form, while other types of valves are mainly used as the pilot stage of multi-stage hydraulic servo valves, including single nozzle baffle valves and double nozzle baffle valves [1].

Electro hydraulic servo valves have strong electromechanical hydraulic coupling, sealing, and structural complexity, making the internal flow channels of the servo valve complex and finely structured. The jet disc, deflection plate, slide valve orifice, and other parts of the valve body are prone to performance degradation and require extremely high processing technology. In addition, the use environment of servo valves is harsh, with a large range of changes in working temperature and medium cleanliness. Its structural construction and use environment limit the improvement of servo valve performance. The decline in the performance of servo valves can lead to numerous defects in hydraulic system control accuracy, slow response, insufficient output pressure and flow rate, which will directly affect the normal operation of hydraulic operating systems and equipment, reduce the service life of equipment, and whether for aircraft or large hydraulic equipment, performance degradation or failure during use may cause irreversible consequences [2].

Therefore, this article proposes a combination of intelligent diagnosis and digital twin for servo valve testing and fault detection. The work done is as follows:

1) Discuss the construction method of servo valve digital twin and the construction of testing system framework. The hardware of the testing system is divided into four main parts: the testing platform, the oil system, the instrument box, and the computer. The digital twin framework includes four stages: three-dimensional twin models, data-driven, dynamic and static testing, and fault diagnosis.

2) The intelligent diagnosis scheme was discussed, and the intelligent diagnosis of faults in electro-hydraulic servo valves can improve diagnostic efficiency and accuracy. In the digital twin testing system of servo valves, a fault diagnosis algorithm based on CNN-LSTM was proposed. CNN was used to fully extract the fault features of the input sequence as the input of LSTM, and LSTM was relied on to fully capture the temporal characteristics of servo valves and identify faults.

3) Set up a simulation experimental environment, analyze and summarize the work done in this article, and verify the feasibility of the method proposed in this article.

2 Related Work

The dynamic and static performance of a servo valve determines its working effect, and the testing of dynamic and static performance is the focus of servo valve research. Therefore, for the research on dynamic and static testing of servo valves, typical results are summarized as follows:

Yong Wang from China Aero Engine Group focused on the static characteristic pressure gain of servo valves, taking the deflection plate jet servo valve as the research object. By establishing a mathematical model of the servo valve machine, electricity, and liquid, a state space model of the electro-hydraulic servo valve was obtained. Then, using the process combined with the pressure gain formula, a first-order sensitivity analysis method was adopted to analyze the correlation and weight of the servo valve structural parameters on the servo valve pressure gain. The improved performance was tested using a testing platform [3].

Xiaoliang Ma from AVIC established a refined mathematical model of the valve controlled motor system, which includes key parameters of the electro-hydraulic servo valve. Then, based on MATLAB/Simulink simulation software, the dynamic characteristics simulation and frequency response analysis of the established system mathematical model were carried out, providing theoretical support and simulation reference for improving the dynamic accuracy and stability of the system and optimizing the structural parameters of the electro-hydraulic servo valve [4].

Yijia Chen proposed a direct acting servo proportional valve structure for the pilot control of the domestically produced DN80 two-way plug-in servo valve to improve its dynamic characteristics. The research process first completed the design of the valve core and sleeve of the direct acting servo proportional valve that matched the flow rate and step response of the DN80 two-way plug-in servo valve, and established a three-dimensional numerical model of the direct acting servo proportional valve. Then, AMEsim software was used to analyze the no-load dynamic characteristics and loaded dynamic characteristics of the direct acting servo proportional valve in detail, and a dedicated large-diameter servo valve test bench was built. Finally, the optimized structure of the direct acting servo proportional valve for the DN80 two-way plug-in servo valve was verified through experiments. The response time has been shortened from 40ms to 23ms, and the dynamic characteristics have been significantly improved [5].

In terms of the design and development of servo valve testing system, Lianjun Shi from Shandong University of Science and Technology has designed a servo valve performance testing system based on virtual instruments, and used this system to complete the measurement of servo valve performance parameters. Compared with traditional servo valve performance testing systems based on VB/CAT, the designed system has the advantages of simple equipment composition, simple programming, high testing accuracy, and good responsiveness, which can reliably complete the main performance testing of servo valves and ensure the safe operation of equipment [6].

Yuan Guo, in order to meet the high requirements of hydraulic cylinder performance testing, developed a LabVIEW based performance testing software for crystallizer vibration servo hydraulic cylinders. The software mainly tests frequency response and step response performance. The performance testing uses sensors to collect displacement and pressure test data, and through an industrial computer, the data is sorted, analyzed, processed, waveform displayed, and stored to achieve real-time measurement and control of performance testing. Through on-site application, it has been verified that the software system has high measurement accuracy, intelligence, and ease of operation, fully meeting the design requirements [7].

In the research process of intelligent diagnosis methods for hydraulic servo valves, Qinghao Zhao from Beijing University of Science and Technology applied big data technology, feature engineering technology, and BP neural network algorithm to extract useful features and patterns. By analyzing the relevant data of servo valves in hot rolling production lines, he designed a servo valve fault analysis model for hot rolling production lines, thereby improving the operating efficiency and reliability of servo systems and providing a reliable monitoring and prediction tool for hot rolling strip enterprises [8].

Shuaiyin Zhang from Shanghai Jiao Tong University proposed a fault diagnosis method based on starfish optimization variational mode decomposition, time-domain convolutional network, and introduction of self attention mechanism for bidirectional gated cyclic units, in response to the limited fault signals that can be collected by the biased jet servo valve and its susceptibility to noise interference, which makes feature extraction difficult. The results showed that the fault recognition accuracy of the proposed model reached 97.33%, with strong robustness and diagnostic accuracy [9].

Yuanhao Hu from Nanjing University of Science and Technology proposed the Attention Convolutional Capsule Network (ACCN) algorithm for the first time to address the problems of unknown parameters and difficulty in modeling in current model-based proportional servo valve fault diagnosis methods. He also designed a new method for proportional servo valve fault diagnosis based on attention convolutional capsule network, which extracts and fuses features from the original multi-channel one-dimensional time-domain signal, and then inputs the fusion result into the subsequent capsule network for feature extraction and fault classification, outputting the corresponding diagnosis result [10].

The composition structure of this article is as follows: Chapter 2 mainly introduces the research results on the fault detection and testing system design of intelligent networks for servo valves. Chapter 3 mainly elaborates on the design process of digital twins and testing system framework. Chapter 4 mainly completes the intelligent diagnosis of faults in electro-hydraulic servo valves and discusses the intelligent diagnosis scheme. Chapter 5 presents the simulation experiment process to prove the effectiveness of the method proposed in this article. Chapter 6 mainly summarizes the research results of this article and plans for further research.

3 Methodology

This chapter mainly discusses the construction methods of digital twins and the construction of testing system frameworks. The hardware of the testing system is divided into four main parts: the testing platform, the oil system, the instrument box, and the computer. The test bench is used to install various instruments, fixtures, hydraulic components; The oil system provides stable oil supply and return for testing and is an important component of the system; The instrument box is equipped with various amplification circuits to sample, amplify, and display flow, pressure, and displacement signals, output valve test signals, and drive working devices such as oil circuit switching control; The computer completes the processing of experimental data and the implementation of human-machine interface [11]. The entire testing process is divided into static testing and dynamic testing parts. In static testing, the computer exchanges data with the secondary instruments of the instrument box. The displacement value of dynamic testing is communicated with the computer through RS232 serial port [12]. The overall design scheme of the system is shown in Fig. 1.

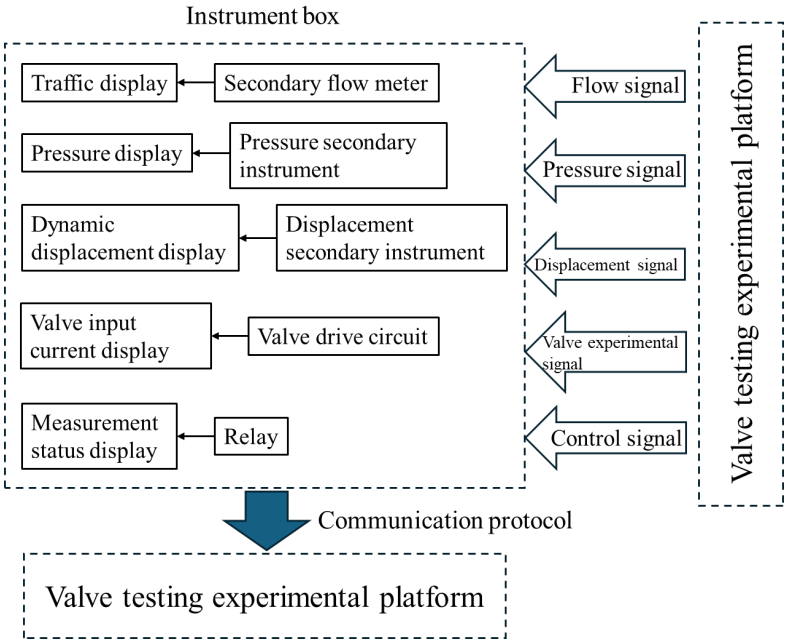

Fig. 1. Overall plan for testing system

According to the testing system plan, construct a digital twin and determine the overall architecture of the system, including the digital twin layer, control layer, execution layer, presentation layer, and research on data transmission protocols and protocols. The control system software can visually view the device status through physical models and digital twin models. Realize dynamic and static performance testing and analysis of servo valves through a digital twin system, as well as intelligent diagnosis of servo valve faults. The work face simulation testing platform project can simulate the actions of equipment on the work face, meeting the simulation testing requirements for automation of work face equipment. The overall framework is shown in Fig. 2.

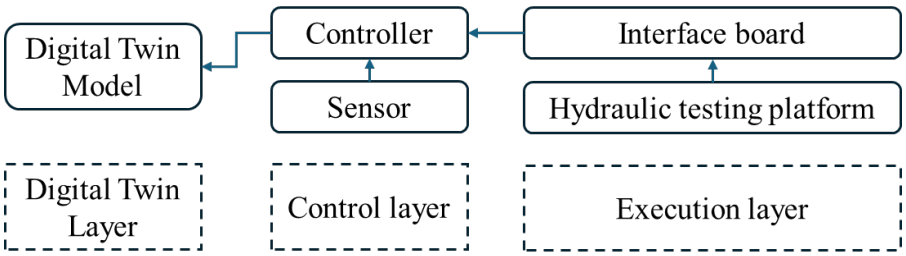

Fig. 2. Overall structure of digital twin testing platform

The main components of the digital twin layer are three-dimensional twin models, data-driven, dynamic and static testing, fault diagnosis, etc. A three-dimensional digital twin model was constructed using virtual electro-hydraulic servo valves and their motion mechanisms. Digital twin data-driven involves data collection, processing, and mapping; Data collection includes communication protocols and information transmission methods, while the data processing stage involves detailed processing of raw data, including data parsing and data exception handling processes. Data mapping is the process of mapping the control layer electro-hydraulic servo data collected by the data twin system to the twin model, enabling the model to accurately describe the dynamic and static characteristics of the servo valve. The overall control layer of the digital twin in the control layer mainly provides functions such as collaborative control logic, data publishing, and remote control interfaces. The data release mainly includes the collection of servo valve sensor information, the internal operation status of the con-

trol system, and the release of control status information, providing digital twin layer subscription. In the digital twin system of hydraulic support, the execution layer provides the support model control input interface and motor drive control, realizing the extension and retraction actions of various components of the servo valve model under the drive of the electric cylinder according to the instructions of the control layer. The execution layer mainly includes the drive control unit, motor drive components, motor actuator, and input detection module. In the actual working environment, the hydraulic source is concentrated in the power supply pump station, the hydraulic support action is controlled by an electro-hydraulic coupling device consisting of an electro-hydraulic directional valve group, and the executing component is a hydraulic cylinder. If the hydraulic support model needs to achieve electric control, it is necessary to drive the control unit to detect the control signal output by the control layer, output the motor control signal, and the motor drive component provides high current output for the motor drive. The motor actuator simulates the action of the oil cylinder to achieve the simulation of the oil cylinder action.

When dealing with digital twin scenarios, it is necessary to simultaneously complete the lightweight processing of components and import the processed components into the development engine. In order to arrange the scene more realistically, a one-to-one comparison arrangement is chosen. After the scene layout is completed, it is necessary to consider adding some constraints and corresponding logic, as well as adding detection techniques at the scene. Real time collision detection can more realistically depict the collision process between objects, promptly detect potential problems that arise during the process, and solve them in a timely manner. As one of the core issues, collision detection requires high-precision real-time monitoring to achieve. However, the complex scene layout poses obstacles to the implementation of this requirement, and it can even be said that real-time detection and high-precision requirements are two opposite scene layouts. Therefore, it is necessary to respond to the requirements reasonably and arrange the scenes according to different practical needs.

The servo valve model consists of three tightly coupled subsystems: an electromagnetic torque motor, a nozzle-flapper assembly, and a hydraulic four-way spool valve. The torque motor at the top converts input current into electromagnetic torque acting on an armature, which in turn actuates a spool valve symmetrically positioned between two opposing nozzles. In equilibrium, the spool valve maintains equal clearance between the two nozzles. However, when the torque motor deflects, it changes the pressure distribution across the nozzles, creating a pressure differential across the spool valve. This pressure imbalance causes the spool valve to move, thereby regulating the hydraulic connection between the supply, return, and load ports. A mechanical feedback lever couples the spool valve motion back to the spool valve, introducing negative feedback to stabilize operation and ensure that spool valve displacement is proportional to the input current. In this way, the valve achieves precise electro-hydraulic conversion, amplifying tiny electrical signals into controlled hydraulic output suitable for high-performance actuation.

3.1 Valve Body Modeling

All parameters used in the model construction process are shown in Table 1.

Table 1. Parameter symbols and their meanings

Parameter symbols	Parameter meaning	Parameter symbols	Parameter meaning
S_{vc}	Valve core displacement	Q_{press}	Servo valve pressure and flow rate
I_{vc}	Valve current	A_{s-val}	Slide valve area
K_{moment}	Mid position electromagnetic torque coefficient of torque motor	k_q	Flow coefficient
K_{am}	Amplifier amplification factor	ρ	Oil density
R_{T-m}	Internal resistance of torque motor coil	T_{elec}	Total electromagnetic torque
R_{am}	Amplifier internal resistance	α	Deflection angle of armature component
l_1	Distance between nozzle axis and torque motor axis	s_{a-noz}	Actual displacement from nozzle center to baffle
l_2	Distance between nozzle axis and slide valve axis	s_{v-rod}	Feedback end virtual displacement

k_{rod}	Feedback bar stiffness	s_t	Minor displacement of the center of mass of the armature component
l_3	Distance from the top of the spring tube to the center of rotation	P_l	Left nozzle pressure
F_{rod}	Feedback power	P_r	Right nozzle pressure
T_{rod}	Feedback torque	g_l	Left zero position gap
J	Moment of inertia of armature rotation	g_r	Right zero position gap
k_{rm-r}	Damping coefficient of armature component rotation	P_{return}	Return oil pressure
k_{rm-m}	Translation damping coefficient of armature component	P_{supply}	Fuel supply pressure
m	Quality of armature	A_l	Left nozzle outlet cross-sectional area
F_q	The liquid flow force at the nozzle hole on the baffle	A_r	Right nozzle outlet cross-sectional area
k_{q-l}	Flow coefficient of left nozzle hole	$q_{s-val-i}$	Valve inlet oil flow rate
k_{q-r}	Right nozzle hole flow coefficient	$q_{s-val-o}$	Valve outlet oil flow rate
k_{q-s-i}	Flow coefficient of inlet valve port	$A_{s-val-r}$	Area of the right end face of the slide valve
k_{q-s-o}	Flow coefficient of return valve port	A_{rod}	Feedback cavity area
$A_{s-val-i}$	Flow area of oil inlet	m_{s-val}	Slide valve quality
$A_{s-val-o}$	Flow area of oil outlet	k_{s-val}	Damping coefficient of slide valve
$P_{s-val-s}$	Oil supply pressure at the spool valve port	$F_{stready}$	steady-state flow force
$P_{s-val-r}$	Return oil pressure of slide valve port	F_{trans}	Transient hydraulic force
$A_{s-val-l}$	Left end face area of slide valve		

Modeling of torque motor, the current signal passes through the control coil to generate control magnetic flux, which interacts with the fixed magnetic flux generated by the permanent magnet at the working air gap to generate electromagnetic torque on the armature, causing the armature to deflect around the center of rotation of the spring tube, thereby driving the movement of the baffle. The electromagnetic torque is expressed as:

$$T_{elec} = K_{moment} \cdot i_c + K_{rod} \cdot \alpha \tag{1}$$

Considering the small displacement x_g of the armature core in the horizontal direction, the armature has two degrees of freedom, rotation and translation. When the armature is subjected to electromagnetic torque, it deflects. Due to the fixed lower end of the spring tube supporting the armature, when the force deforms, the actual displacement at its top can be expressed as:

$$s_a = s_t + l_3 \cdot \alpha \tag{2}$$

The actual displacement of the nozzle hole center facing the baffle and the virtual displacement of the feedback rod end can be expressed as:

$$s_{a-noz} = l_1 \cdot \alpha - s_t \tag{3}$$

$$s_{v-rod} = \left(l_1 + l_2\right) \cdot \alpha - s_a \tag{4}$$

The feedback force of the feedback bar is expressed as:

$$F_{kod} = k_{rod}\left(s_a - s_{v-rod}\right) \tag{5}$$

For the armature component, considering both translational and rotational degrees of freedom, the force balance equation is:

$$\begin{cases} T_{elec} = J\dfrac{d^2\alpha}{dt^2} + k_{arm-r}\cdot\dfrac{d\alpha}{dt} + F_{rod}\cdot\left(l_1 + l_2\right) + F_q\cdot l_1 \\ F_q + F_{rod}\left(l_1 + l_2\right) = m\cdot\dfrac{d^2 s_t}{dt^2} + k_{rm-m}\dfrac{ds_t}{dt} \end{cases} \tag{6}$$

Nozzle modeling, the oil flowing through the nozzle acts on the surface of the baffle, and the baffle surface is subjected to the force of the oil in the nozzle cavity, which is called the fluid flow force. This force is composed of the hydraulic force caused by the static pressure and momentum changes of the oil. According to the Bernoulli equation, the fluid flow forces acting on the left and right sides of the baffle are respectively expressed as:

$$F_{q-l} = P_l + \frac{16\left(g_l - s_{a-noz}\right)^2\cdot k_{q-l}\left(P_l - P_{return}\right)}{A_l} \tag{7}$$

$$F_{q-r} = P_r + \frac{16\left(g_r - s_{a-noz}\right)^2\cdot k_{q-r}\left(P_r - P_{return}\right)}{A_r} \tag{8}$$

The flow rate expressions for the left and right nozzles are as follows:

$$q_l = k_{q-l}\cdot\pi\cdot A_l\left(g_l - s_{a-noz}\right)\sqrt{\frac{2\left(P_l - P_{return}\right)}{\rho}} \tag{9}$$

$$q_r = k_{q-r}\cdot\pi\cdot A_r\left(g_r - s_{a-noz}\right)\sqrt{\frac{2\left(P_r - P_{return}\right)}{\rho}} \tag{10}$$

The modeling of the slide valve component takes into account the radial clearance at the slide valve and the rounded corners of the valve core and sleeve. The slide valve adopts a three-way valve structure with a positive overlap, and only one valve port is open at the same time for the inlet and return ports. Due to the presence of radial clearance, the flow state of the closed valve port is an annular gap. According to the flow rate formula of the valve port and the flow rate formula of the annular gap flow, the flow rates of the inlet and return valve ports can be obtained:

$$q_{s-val-i} = \begin{cases} k_{q-s-i}\cdot A_{s-val-i}\sqrt{\dfrac{2}{\rho}\left(P_{s-val-s} - P_{out}\right)} & s_a \geq c_{in} \\ \dfrac{\pi\left(P_{s-val-s} - P_{out}\right)}{12\mu\left(c_{in} - s_a\right)} & s_a < c_{in} \end{cases} \tag{11}$$

$$q_{s-val-o} = \begin{cases} k_{q-s-o}\cdot A_{s-val-o}\sqrt{\dfrac{2}{\rho}\left(P_{out} - P_{s-val-r}\right)} & s_a \leq c_{out} \\ \dfrac{\pi\left(P_{out} - P_{s-val-r}\right)}{12\mu\left(s_a - c_{out}\right)} & s_a > c_{out} \end{cases} \tag{12}$$

The spool is subjected to hydraulic pressure, inertial force, viscous damping force, feedback rod reaction force on the spool, spool hydraulic force, and hydraulic pressure of the feedback chamber oil during its movement. Therefore, the dynamic equation of the spool valve can be obtained as:

$$A_{s-val-l}P_l - A_{s-val-r}P_r - A_{rod}P_{out} = m_{s-val}\frac{d^2 s_a}{dt^2} + k_{s-val}\frac{ds_a}{dt} + F_{steady} + F_{trans} \tag{13}$$

3.2 Principle of Dynamic and Static Performance Testing

The digital twin dynamic and static testing system constructed in this article is mainly aimed at testing the dynamic and static performance of electro-hydraulic servo valves. The static performance includes pressure flow characteristics (load flow characteristics), no-load flow characteristics, pressure characteristics, internal leakage characteristics.

The pressure flow characteristic curve is used to determine the type of servo valve and estimate its specifications to match the required load flow rate and load pressure. The transfer function of a servo valve (force feedback two-stage servo valve, actual frequency>50 Hz) under static conditions is expressed as:

$$\frac{S_{vc}}{I_{vc}} = \frac{2 \cdot K_{moment} \cdot K_{am}}{\left(R_{T-m} + R_{am}\right)\left(l_1 + l_2\right) \cdot k_{rod}} \tag{14}$$

In the formula, S_{vc} represents the displacement of the valve core, I_{vc} represents the valve current, K_{moment} represents the median electromagnetic torque coefficient of the torque motor, K_{am} represents the amplification factor of the amplifier, R_{T-m} is the internal resistance of the torque motor coil, R_{am} represents the internal resistance of the amplifier, l_1 represents the distance between the nozzle axis and the torque motor axis, and l_2 represents the distance between the nozzle axis and the spool valve axis. K_{rod} represents the stiffness of the feedback bar. Therefore, the static voltage balance equation of the torque motor is expressed as:

$$K_{am} \cdot I_{vc} = \left(R_{T-m} + R_{am}\right) \cdot i_c / 2 \tag{15}$$

i_c represents the control current of the electro-hydraulic servo valve, therefore, under static conditions:

$$S_{vc} = \frac{K_{moment} \cdot i_c}{\left(l_1 + l_2\right) \cdot k_{rod}} \tag{16}$$

The pressure flow characteristic equation of the servo valve is expressed as:

$$Q_{press} = k_q \cdot A_{s-val} \frac{K_{moment} \cdot i_c}{\left(l_1 + l_2\right) \cdot k_{rod}} \sqrt{\frac{P_{\text{supply}} - P_{return}}{\rho}} \tag{17}$$

The no-load flow curve is a function curve of the output flow rate and input current forming a loop shape. It not only gives the polarity, rated no-load flow rate, and nominal flow gain of the valve, but also obtains the linearity, symmetry, hysteresis, resolution of the valve, and reveals the zero zone characteristics of the valve. The relationship between the flow rate from the return port of an electro-hydraulic servo valve and the control current when the output flow rate is zero and the supply pressure is constant. The internal leakage characteristics vary with the input current and are maximum when the valve is in the zero position.

This article mainly tests the dynamic characteristics of electro-hydraulic servo valves. The system is excited by a sine signal with a known frequency, and the steady-state response signal of the system is measured. The dynamic characteristics of the system are defined by the transfer function composed of the amplitude ratio and phase difference between the output and input. By changing the frequency point, the frequency response of other points can be measured.

Assuming the transfer function of the servo valve is expressed as:

$$C_{sv}(j\omega) = C_{sv}(s)\big|_{s=j\omega} \tag{18}$$

The step response excitation signal is shown in Fig. 3.

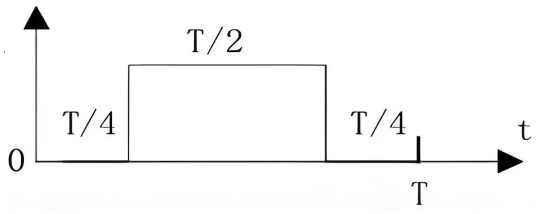

Fig. 3. Step response excitation signal

When performing autocorrelation processing on sine signals, the initial phase information β inherent in them does not appear in the correlation function, which means that the phase information of the original harmonic signal is lost during autocorrelation processing. However, when performing cross-correlation processing on two sine signals of the same frequency, the phase difference $\Delta\beta$ between the two sine waves appears in the cross-correlation function. Therefore, the phase difference information between the two sine signals is retained during cross-correlation processing. And during the intermittent time shift value $r = 0$:

$$R_{xy}(0) = \frac{AB}{2}\cos\beta \tag{19}$$

During testing, the servo valve inputs a sine current signal, which is represented as:

$$i(t) = X_i \sin\left(\omega t + \delta_i(\omega)\right) \tag{20}$$

When performing constant amplitude frequency conversion within a certain frequency range, when the system reaches steady state, the output signal is a sine signal with the same frequency but varying amplitude and phase:

$$i_o(t) = X_o \sin\left(\omega t + \delta_o(\omega)\right) \tag{21}$$

The amplitude frequency characteristics of the servo valve can be expressed as follows:

$$A_{sv}(\omega) = 20\log\left|\frac{X_o(\omega)}{X_i(\omega)}\right| \tag{22}$$

The phase frequency characteristic is the difference in phase between the input current of a servo valve measured at a certain frequency and its corresponding output flow rate:

$$\delta(\omega) = \delta_o(\omega) - \delta_i(\omega) \tag{23}$$

The schematic diagram of the testing principle is shown in Fig. 4.

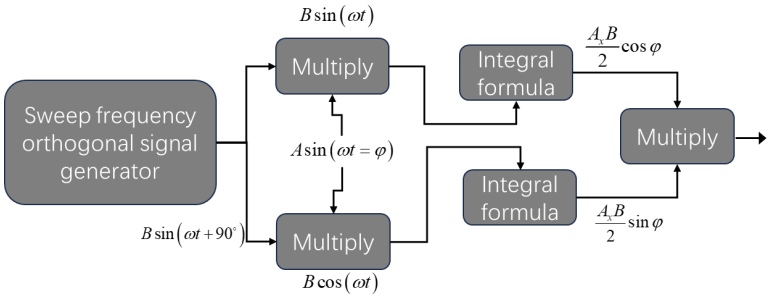

Fig. 4. Schematic diagram of testing principle

The above has completed the construction of the framework and structural principles for the digital twin testing system.

4 Intelligent Diagnosis Method for Faults in Electro-Hydraulic Servo Valves

The intelligent diagnosis of faults in electro-hydraulic servo valves can improve diagnostic efficiency and accuracy. Therefore, in the digital twin system of servo valves, a fault diagnosis scheme is added. This section mainly discusses the intelligent diagnosis scheme.

A fault diagnosis algorithm based on CNN-LSTM was proposed, which utilizes CNN [13] to fully extract the fault features of the input sequence as the input of LSTM [14], and relies on LSTM to fully capture the temporal characteristics of the servo valve.

Use linear normalization method to preprocess the input pressure data. The processing method is as follows:

$$x_{lin-nor} = \frac{x - x_{\min}}{x_{\max} - x_{\min}} \tag{24}$$

In the equation, $x_{\min}$ and $x_{\max}$ represent the minimum and maximum values in the input sequence. The loss function is represented by the Cross Entropy Loss function as follows:

$$CE\left(y, y^p\right) = \sum_{i=1}^{N} y_i \log\left(y_i^p\right) \tag{25}$$

N represents the number of samples, y_i is the probability of the actual label being the i-th category, and y_p^i is the probability of the i-th category output by the network model. LSTM adds three threshold controllers to its structure, namely input gate, forget gate, and output gate. The hidden layer state from the previous moment is passed to the forget gate, input gate, and output gate, allowing the network model to selectively remember the input data and efficiently learn the temporal dependencies between data. The structure of the model memory unit is shown in Fig. 5.

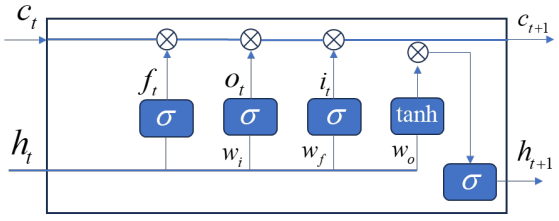

Fig. 5. Structure diagram of model memory unit

LSTM contains two iterative lines, one of which ultimately outputs the state of the hidden layer [15]. At the same time, another line indicates that the iteration is completed by filtering information through the forget gate and input gate [16], and finally the cell state of the hidden layer at time t is generated following the output gate. The output of the forget gate is represented as:

$$f_{out} = f_{sigmoid}\left(\lambda_{connect}\left[s_{t-1}, f_{in}\right] + b_f\right) \tag{26}$$

In the equation, $[s_{t-1}, f_{in}]$ represents the vector connecting the previous hidden layer state s_{t-1} and the current input f_{in}, $\lambda_{connect}$ represents the weight, and b_f represents the bias.

By utilizing CNN to fully extract local features of the input sequence, the fault features of the electro-hydraulic servo valve are extracted [17]. Then, the output of CNN is passed to LSTM, which fully mines the temporal information in the CNN output to extract the fault features of the electro-hydraulic servo valve in the time dimension. Finally, fault classification is performed through a fully connected layer, the structure of the lower branch is basically the same as that of the upper branch [18], and a learnable offset is introduced to adapt to the non-stationary characteristics of the signal. The representation method is as follows:

$$y(p) = \sum_{n=1}^{m} w_n \cdot x_g\left(p_k + \Delta p_k\right) \tag{27}$$

p_k represents the learning offset, which increases the flexibility of CNN and improves its recognition ability.

5 Experimental Results and Discussion

A digital twin monitoring and fault diagnosis system for landing gear health management was designed and implemented based on the C/S (Client/Server) architecture. At the system development level, Python 3.10 is chosen as the core programming language, mainly based on its rich scientific computing library and ecological advantages of machine learning frameworks. The software environment adopts the Windows 10 operating system, and the development tools use the Visual Studio Code 2022 integrated development environment. The system uses Pyside6 to build the client GUI interface, and SQLite database is selected as the database. The overall architecture is shown in Fig. 6.

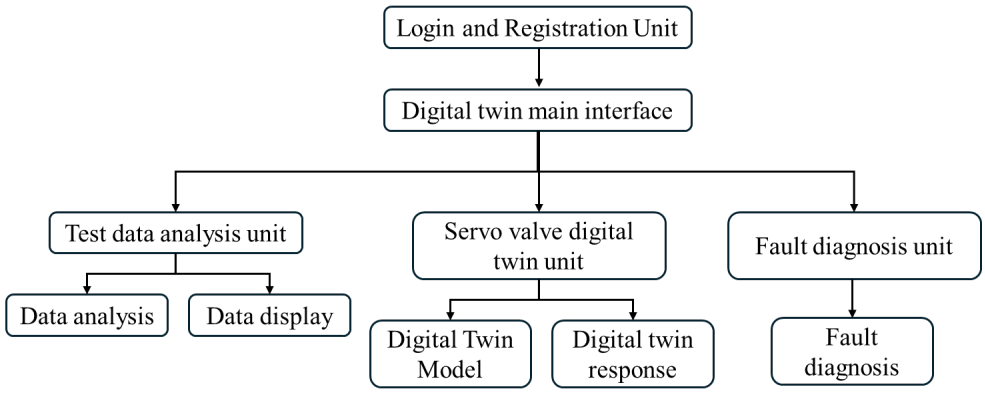

Fig. 6. Overall system block diagram

In terms of interface design, the team use the QWWidget provided by Pyside6 as the main window container and utilize QVBoxLayout and QGridLayout for control layout management. The core elements of the interface include two QLabels for displaying prompt text for “username” and “password”, two QLineEdits for receiving user input, and two QPushButtons for login and registration functions. The interface color scheme adopts a black

and white theme, and the control is beautified through a style sheet to ensure a simple and beautiful interface. In terms of database integration, the system uses SQLite as the backend database and utilizes the built-in SQLite3 module in Python for database operations. A user information table has been designed in the database, which includes fields such as username and password.

After entering the dynamic and static testing system, Fig. 7 shows a two-dimensional Cartesian plot designed to illustrate the ideal linear relationship and the effects of noise or perturbations on the measurement. The horizontal and vertical axes are symmetrically distributed, ranging from -12.5 to +12.5, with evenly spaced tick marks to provide a consistent scale. The plot area is displayed with a white background, a green dashed grid, and a black background to enhance the visual clarity of the plot. Three noteworthy graphical elements can be observed in the plot. First, a solid red diagonal line extends from the lower left corner (10, 10) to the upper right corner (10, 10). This line passes through the origin and has a slope of approximately 1, representing the reference function $y = x$. This diagonal line represents the ideal or nominal relationship between input and output values, which can be compared to the deviation. Second, the plot contains a dense band of red scattered points distributed horizontally across the entire range of $x \in [10, 10]$. These points are tightly clustered near $y \approx 0$, forming a noise cloud that can be described as near-zero. The scatter plot illustrates how measured or simulated data can fluctuate randomly around a baseline despite the presence of an ideal linear trend. These points are numerous and densely packed together so that they form a seemingly continuous horizontal stripe, reflecting the persistence of small, unbiased variations [19]. Importantly, this noise stripe intersects a reference diagonal line near the origin, emphasizing the contrast between the ideal functional relationship and real-world perturbations. Third, the plot includes a vertical blue dashed line located exactly at $x = 0$. This line serves as a reference marker, bisecting the plot, focusing attention on the central axis and emphasizing the origin's role as an axis of symmetry. The inclusion of this line further enhances the interpretability of the plot by clarifying the alignment of the red diagonal line and the noise horizontal stripe relative to the coordinate center. Overall, the plot provides a multi-layered visualization: the red diagonal line represents the theoretically perfect input-output mapping, the dense horizontal scatter band indicates random variations in practice that can mask this ideal mapping, and the vertical blue dashed line highlights the central reference point for comparison. This visualization is often used in error analysis, control system testing, or signal processing demonstrations, where the interaction between an ideal model and noisy observations is of central interest [20]. By combining reference geometry, noise visualization, and axis labeling, the plot conveys the robustness of the ideal relationship while alerting the observer to the inevitable fluctuations in real-world data.

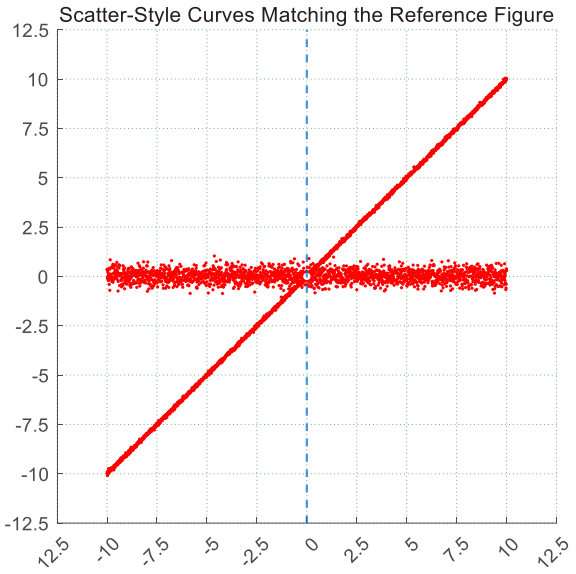

Fig. 7. Static test results

This Fig. 8 shows a two-dimensional plot with a logarithmic x-axis and a linear y-axis. This plot is commonly used to visualize dynamic system responses, frequency-domain data, or error growth across multiple orders of

magnitude [21]. The horizontal (x-axis) scale is logarithmic, ranging from 1 to approximately 1000. This scaling enables the plot to capture fine-grained behavior at small input values and large-scale trends at larger magnitudes, which would otherwise be compressed in a linear plot. The vertical (y-axis) ranges from approximately 0 at the top to -300 at the bottom, providing a wide range for examining signal amplitude or error magnitude. The red curve represents the primary data set. Initially, for small x-values (close to 1), the curve remains relatively stable, with slight fluctuations around -50. As x-values increase to approximately 10-100, the red curve begins to gradually decline, indicating a shift in the system dynamics. Beyond this region, especially as x approaches and exceeds 100, the curve exhibits a sharp decline, accompanied by large fluctuations. This noisy region indicates instability or high variability at higher input scales, a behavior often associated with increasing uncertainty, numerical instability, or physical limitations of the modeled system. A vertical blue line is drawn near x=100. This line acts as a threshold marker, separating the more stable portion of the curve on the left from the highly variable region on the right. It may represent a cutoff frequency, a critical iteration exponent, or a boundary condition beyond which the system behavior becomes unpredictable. The bidirectional grid lines provide additional clarity, especially the logarithmic scale along the x-axis, which highlights the exponential scaling of the input domain. Overall, the plot conveys three stages of behavior in the red signal: (1) a stable region at low values, (2) a transitional drop-off, and (3) a high-variance, unstable region beyond the blue threshold. This type of plot is particularly suitable for illustrating the robustness and eventual breakdown of control algorithms, signal filters, or numerical approximation methods as the input or iteration scale increases.

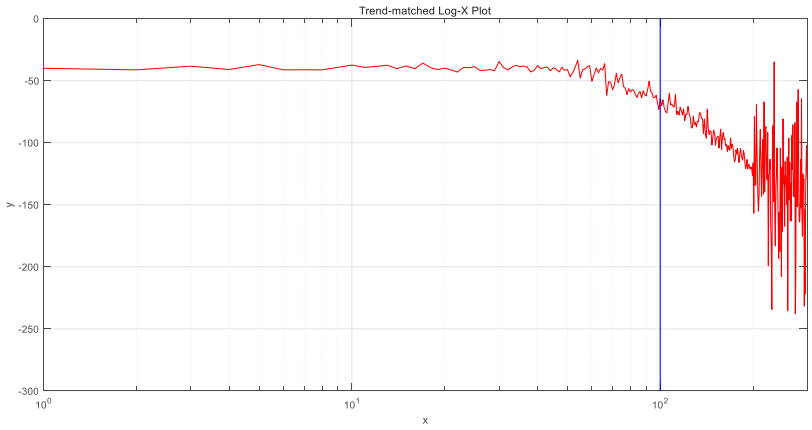

Fig. 8. Frequency response characteristic curve

This Fig. 9 shows a line chart of the accuracy of a deep learning model on the training and test sets after 50 epochs of training. The horizontal axis represents the epoch number, ranging from 0 to 50; the vertical axis represents the percentage of classification accuracy, ranging from 0% to 100%. The solid orange line represents the accuracy achieved on the training set, and the dashed dark blue line represents the accuracy achieved on the test set. In the early stages of training (the first five epochs), both curves show relatively low accuracies, approximately 30% on the test set and slightly above 40% on the training set. Within the first 10-15 epochs, both curves show a rapid upward trend, indicating that the model quickly learns the basic representation of the data and has considerable generalization ability. After 15 epochs, the training accuracy continues to climb, fluctuating between 95% and 100%, reflecting a near-perfect fit between the model and the training data. While the test accuracy is slightly lower, it stabilizes between 90% and 95% after 15 epochs and fluctuates only slightly as training progresses. This demonstrates that the model maintains strong generalization capabilities to unseen data. The small but consistent gap between the training and test curves highlights some degree of overfitting; the model performs slightly better on the training set than on the test set, but the difference is small and within an acceptable range. Overall, the graph demonstrates effective model learning: rapid initial convergence, high final training accuracy, and stable test accuracy. These trends suggest that the lightweight architecture and training strategy strike a balance between learning and generalization capabilities, avoiding catastrophic overfitting or underfitting [22].

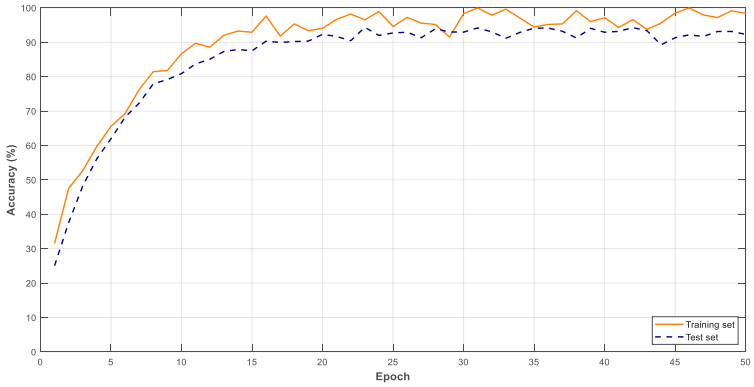

Fig. 9. Algorithm iteration effect

Fig. 10 shows a comparative analysis of the model accuracy of two architectures over 50 epochs of training: a CNN-LSTM hybrid model (solid orange line) and a standard CNN (dashed blue line). The horizontal axis represents the epoch number, and the vertical axis represents classification accuracy (%), ranging from 20% to 100%. Initially, both models achieve relatively low accuracy (around 30%), reflecting the difficulty of the task with randomly initialized parameters. Within the first 10 epochs, the CNN-LSTM demonstrates a more pronounced improvement, exceeding 70% accuracy, while the CNN lags slightly behind. Between epochs 10 and 20, the CNN-LSTM continues to outperform the CNN, reaching an accuracy approaching 90%, while the CNN maintains a stable accuracy between 80% and 85%. This demonstrates that the recurrent structure of the LSTM provides additional capacity to capture temporal dependencies or sequence characteristics that a standalone CNN cannot fully exploit. After epoch 20, the two models begin to converge and stabilize, with the CNN-LSTM maintaining a slight but consistent advantage. Accuracy fluctuations are more pronounced, especially in the CNN-LSTM curve, likely due to that model's greater sensitivity to training dynamics. Despite this, the CNN-LSTM consistently maintains higher peak accuracy, fluctuating around 90-92%, while the CNN peaks at approximately 87-90%. Overall, this graph highlights the advantage of hybrid CNN-LSTM architectures for tasks requiring richer temporal or contextual feature extraction, as they not only achieve faster early convergence but also maintain higher accuracy later in training. While the CNN model is simpler and more stable, it has a slightly lower performance ceiling, demonstrating the trade-off between architectural complexity and raw predictive power [23].

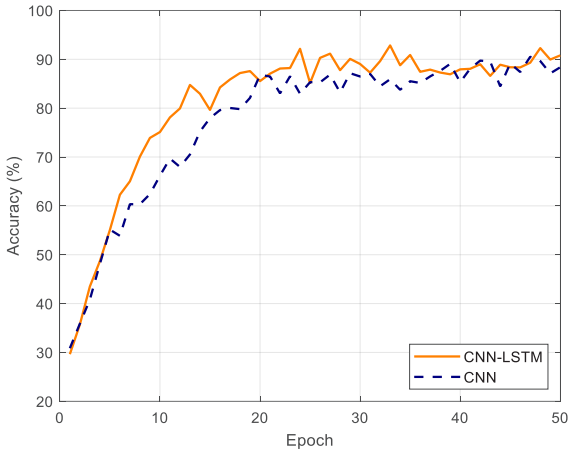

Fig. 10. Comparison results of accuracy before and after improvement

6 Conclusion

The conclusions of this study highlight that the signal generators, frequency response analyzers, and associated recording instruments traditionally used for dynamic and static testing of electro-hydraulic servovalves have been successfully virtualized and integrated into a digital twin framework. This innovation significantly reduces reliance on expensive physical hardware, thereby lowering system costs, simplifying experimental setup, and increasing operational flexibility. By embedding these testing capabilities within the digital twin, researchers were able to simulate, measure, and record the necessary signals in a fully virtual environment while maintaining fidelity that meets engineering and research standards. During the pressure-flow characteristic testing experiments, a digital filtering module was applied to the raw measurement signals. This process effectively attenuated noise and smoothed fluctuations, bringing the measured curve closer to the ideal theoretical curve. The improved agreement between the measured and theoretical outputs validates the use of digital filtering as a key step in improving the accuracy and reliability of servovalves testing, ensuring that the experimental data can be reliably used for system modeling and fault analysis. Furthermore, the static pressure gain test procedure has been improved, utilizing a point-by-point measurement method rather than relying solely on continuous sweeps or approximate data interpolation. This improvement increases the resolution of the test results, enabling more accurate characterization of the servovalves' static performance parameters. Importantly, the improvements in this method are not limited to pressure gain testing but can be extended to other static performance assessments, such as leakage, symmetry, and hysteresis, making it widely applicable to servovalve research. Despite these advances, some limitations remain. Specifically, during pressure and flow testing experiments, the load conditions at the servovalve's A and B ports must currently be manually adjusted. This manual operation introduces a degree of human variability and potential errors, which impacts the repeatability and accuracy of the results. The reliance on operator skill and real-time judgment also limits the scalability of the test system for long-term or batch experiments. To address this limitation, the use of proportional throttle valves for load adjustment is proposed. These valves can be integrated into the digital twin control loop, automatically adjusting the load via computer commands without the need for human intervention. This upgrade will enable precise, repeatable, and finely adjustable load adjustment while minimizing human intervention. By automating the load control process, the overall intelligence and autonomy of the system will be significantly enhanced, enabling the test platform to provide not only more accurate but also more consistent results across repeated experiments. While digital twin-based systems already offer significant advantages in reducing costs, improving test accuracy, and increasing experimental efficiency, the addition of automated proportional throttle valve control represents a logical next step in their evolution. This advancement will propel the test platform toward full automation, reduce experimental uncertainty, and enable more comprehensive and precise evaluation of servovalve performance under a variety of realistic operating conditions.

7 Acknowledgement

Funded by Platform Project: Horizontal Project: Design and Development of Servo Valve Dynamic and Static Test Bench (Project No.: Heng 20250027).

References

[1] S. Kang, H. Yan, C.-C. Li, Research review of the deflector jet servo valve, Journal of Beijing Jiaotong University 41(1) (2017) 130-139.
https://doi.org/10.11860/j.issn.1673-0291.2017.01.020

[2] Q. Guo, Development of Nonlinear Control Technology for Electro-hydraulic Servo System, Chinese Hydraulics & Pneumatics (3)(2018) 1-9.
https://doi.org/10.11832/j.issn.1000-4858.2018.03.001

[3] Y. Wang, D. Zhang, C.-K. Yang, X.-D. Liu, W. Gao, X.-D. Li, Sensitivity Analysis of Influencing Factors on Pressure Gain of Electro-hydraulic Servo Valve, Chinese Hydraulics & Pneumatics 48(7)(2024) 53-62.
https://doi.org/10.11832/j.issn.1000-4858.2024.07.006

[4] X.-L. Ma, Y.-B. Wang, J.-Y. Yuan, H.-H. Yang, Y.-L, Jiang, Modeling and Dynamic Characteristic Analysis of Radar Turntable Valve-controlled Motor System, Hydraulics Pneumatics & Seals 44(12)(2024) 32-38.
https://doi.org/10.3969/j.issn.1008-0813.2024.12.006

[5] Y.-J. Chen, D.-S. Chen, G. Lin, J.-Y. Zhao, G.-J. Jin, B. Chen, Dynamic Characteristics Research and Structural Optimization Design of Direct Acting Servo Proportional Valve, Metallurgical Equipment (1)(2023) 1-6. https://doi.org/10.3969/j.issn.1001-1269.2023.01.001
[6] L.-J. Shi, L. Zhu, H.-Z. Shi, Design and Implementation of Servo Valve Test System Based on Virtual Instrument, Machine Tool & Hydraulics 50(19)(2022) 66-72. https://doi.org/10.3969/j.issn.1001-3881.2022.19.012
[7] Y. Guo, S.-X. Li, J. Tan, L. Wu, Development of Dynamic Performance Testing Software for Mold Vibration Servo Hydraulic Cylinder, Hydraulics Pneumatics & Seals 44(3)(2024) 53-57. https://doi.org/10.3969/j.issn.1008-0813.2024.03.010
[8] Q.-H. Zhao, F.-W. Jing, Fault Analysis Method of Hot Rolling Production Line Servo Valve Based on BP Neural Network Algorithm, Metrology & Measurement Technique 50(12)(2024) 113-117. https://doi.org/10.15988/j.cnki.1004-6941.2024.12.033
[9] S.-Y. Zhang, J.-F. Tao, Z.-Y. Wu, F.-F.-Y. Chen, H.-Y. Tan, Fault Diagnosis of Deflector Jet Servo Valve Based on Variational Mode Decomposition and Bidirectional Gated Recurrent Unit, Chinese Hydraulics & Pneumatics 49(8)(2025) 1-11. https://doi.org/10.11832/j.issn.1000-4858.2025.08.001
[10] Y.-H. Hu, Y.-B. Song, J.-H. Liu, X.-L. Zhao, W.-X. Deng, J. Hu, J.-Y. Yao, Fault diagnosis of electro-hydraulic proportional servo valves based on attention convolutional capsule networks, Acta Aeronautica et Astronautica Sinica 45(15)(2024) 630407. https://doi.org/10.7527/S1000-6893.2024.30407
[11] Y. Gao, Research on verification device for electro-hydraulic control system of hydraulic support in full working face, Mining & Processing Equipment 51(12)(2023) 1-7. https://doi.org/10.3969/j.issn.1001-3954.2023.12.001
[12] S.-H. Wei, Design of an Integrated Testing Platform for Aircraft Hydraulic/Landing Gear Systems, Automation & Instrumentation 40(1)(2025) 100-103+108. https://doi.org/10.19557/j.cnki.1001-9944.2025.01.020
[13] M.-H. Liu, J.-B. Xiong, N.-Q. Su, C.-L. Li, J. Cen, Y.-Y. Zhang, Review of Bearing Fault Diagnosis of Petrochemical Units Based on Deep Learning, Machine Tool & Hydraulics 51(6)(2023) 171-180. https://doi.org/10.3969/j.issn.1001-3881.2023.06.031
[14] L.-Y. Chai, H.-Y. Luan, Z.-Y. Liu, Z. Shen, X. Ren, Long Short-term Memory Prediction Anti-disturbance Backstepping Control of Valve Controlled Hydraulic Motor Position Servo System, Chinese Hydraulics & Pneumatics 48(8)(2024) 128-136. https://doi.org/10.11832/j.issn.1000-4858.2024.08.014
[15] G.-B. Huang, Y.-Q. Chen, H.-A. Babri, Classification Ability of Single Hidden Layer Feedforward Neural Networks, IEEE Transactions on Neural Networks 11(3)(2000) 799-801. https://doi.org/10.1109/72.846750
[16] D. Shen, Iterative Learning Control with Incomplete Information: A Survey, IEEE/CAA Journal of Automatica Sinica 5(5)(2018) 885-901. https://doi.org/10.1109/JAS.2018.7511123
[17] S. Sharifi, A. Tivay, S.-M. Rezaei, M. Zareinejad, B. Mollaei-Dariani, Leakage Fault Detection in Electro-Hydraulic Servo Systems Using a Nonlinear Representation Learning Approach, ISA Transactions 73(2018) 154-164. https://doi.org/10.1016/j.isatra.2018.01.015
[18] P. Cui, M.-K. Wu, H.-J. Lu, Y.-J. An, Z. Cao, X.-W. Feng, R.-Z. Ma, Fault diagnosis of converter transformers based on time-frequency maps and parallel CNN−LSTM, Ningxia Electric Power (4)(2025) 53-59+66. https://qikan.cqvip.com/Qikan/Article/Detail?id=7201643373
[19] M. Vojta, Lattice Symmetry Breaking in Cuprate Superconductors: Stripes, Nematics, and Superconductivity, Advances in Physics 58(6)(2009) 699-820. https://doi.org/10.1080/00018730903122242
[20] M. Rautenhaus, M. Böttinger, S. Siemen, R. Hoffman, R.-M. Kirby, M. Mirzargar, N. Röber, R. Westermann, Visualization in Meteorology—A Survey of Techniques and Tools for Data Analysis Tasks, IEEE Transactions on Visualization and Computer Graphics 24(12)(2018) 3268-3296. https://doi.org/10.1109/TVCG.2017.2779501
[21] D. Petri, D. Fontanelli, D. Macii, A Frequency-Domain Algorithm for Dynamic Synchrophasor and Frequency Estimation, IEEE Transactions on Instrumentation and Measurement 63(10)(2014) 2330-2340. https://doi.org/10.1109/TIM.2014.2308996
[22] M.-M. Bejani, M. Ghatee, A Systematic Review on Overfitting Control in Shallow and Deep Neural Networks, Artificial Intelligence Review 54(8)(2021) 6391-6438. https://doi.org/10.1007/s10462-021-09975-1
[23] C.-N. Clark, A. Bedada, B. Huff, B. Lita, A.-B. Newbury, F. Pacifici, Investigating the Resolution-Performance Trade-off of Object Detection Models in Support of The Sustainable Development Goals, IEEE Journal of Selected Topics in Applied Earth Observations and Remote Sensing 16(2023) 5695-5713. https://doi.org/10.1109/JSTARS.2023.3284309